REVIEW

Advances in laser speckle imaging: From qualitative to quantitative hemodynamic assessment

Muhammad Mohsin Qureshi[1] 🆔 | **Nader Allam**[1,2] | **Jeongmyo Im**[3] |
Hyuk-Sang Kwon[3] | **Euiheon Chung**[3,4] | **I. Alex Vitkin**[1,2,5]

[1]Division of Biophysics and Bioimaging, Princess Margaret Cancer Centre, University Health Network, Toronto, Canada

[2]Department of Medical Biophysics, University of Toronto, Toronto, Canada

[3]Department of Biomedical Science and Engineering, Gwangju Institute of Science and Technology, Gwangju, Republic of Korea

[4]AI Graduate School, Gwangju Institute of Science and Technology, Gwangju, Republic of Korea

[5]Department of Radiation Oncology, University of Toronto, Toronto, Canada

Correspondence
Muhammad Mohsin Qureshi, Division of Biophysics and Bioimaging, Princess Margaret Cancer Centre, University Health Network, Toronto M5G 1L7, Canada.
Email: mohsin.qureshi2@uhn.ca

Euiheon Chung, Department of Biomedical Science and Engineering, Gwangju Institute of Science and Technology, Gwangju 61005, Republic of Korea.
Email: ogong50@gist.ac.kr

I. Alex Vitkin, Division of Biophysics and Bioimaging, Princess Margaret Cancer Centre, University Health Network, Toronto M5G 1L7, Canada.
Email: vitkin@uhnres.utoronto.ca

Abstract

Laser speckle imaging (LSI) techniques have emerged as a promising method for visualizing functional blood vessels and tissue perfusion by analyzing the speckle patterns generated by coherent light interacting with living biological tissue. These patterns carry important biophysical tissue information including blood flow dynamics. The noninvasive, label-free, and wide-field attributes along with relatively simple instrumental schematics make it an appealing imaging modality in preclinical and clinical applications. The review outlines the fundamentals of speckle physics and the three categories of LSI techniques based on their degree of quantification: qualitative, semi-quantitative and quantitative. Qualitative LSI produces microvascular maps by capturing speckle contrast variations between blood vessels containing moving red blood cells and the surrounding static tissue. Semi-quantitative techniques provide a more accurate analysis of blood flow dynamics by accounting for the effect of static scattering on spatiotemporal parameters. Quantitative LSI such as optical speckle image velocimetry provides quantitative flow velocity measurements, which is inspired by the particle image velocimetry in fluid mechanics. Additionally, discussions regarding the prospects of future innovations in LSI techniques for optimizing the vascular flow quantification with associated clinical outlook are presented.

KEYWORDS
2D angiography, biophotonics, blood flow measurement, laser speckle, qualitative, quantitative, semi-quantitative
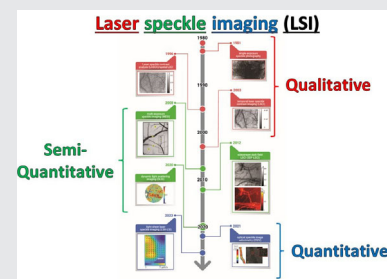
1 | INTRODUCTION

Microvascular structures consist of arterioles, metarterioles (precapillary arterioles), capillaries, and venules, whose functionality has paramount importance in tissue perfusion that enables oxygenation and the transport of vital metabolites to and from the tissue [1]. In particular, blood flow within the microvasculature where such biochemical exchanges predominantly occur is an essential physiological parameter that directly impacts the health and homeostasis of the associated organs and tissues [2, 3]. Therefore, the functional status of microvascular flow is crucial in the characterization of numerous diseases which are associated with compromised blood perfusion, including stroke [4, 5], Alzheimer's disease, and other dementias [6–8], cardiovascular diseases [9], cancer [10], coronavirus infections [11], and many others [12, 13]. Specifically, longitudinal monitoring of the changes in microcirculation can be used to determine the disease progression and treatment efficacy of potential therapeutics. In this regard, much of the previous preclinical research has been directed to elucidate the role of microcirculation in disease progression and focused on the quantification of microvascular perfusion for clinical applications in therapy developments and response monitoring.

Over the past few decades, enabled in large part by the advances in laser and associated photonics technology, multiple breakthroughs in novel optical imaging and microscopy techniques have been introduced for quantifying blood flow in *in vivo* settings, often at resolutions unreachable by other angiography modalities [14]. These include optical coherence tomography (OCT) [15, 16], two-photon microscopy (TPM) [17, 18], laser Doppler flowmetry [19], photoacoustic Doppler [20], red blood cell (RBC) tracking measurements [21], confocal laser scanning microscopy [22, 23], and laser speckle imaging (LSI) [24, 25]. Table 1 shows the comparison of LSI and other optical modalities. All these techniques, as well as several non-optical approaches not mentioned here, have their pros and cons as summarized in several recent publications [34–36]. In this review, we focus on microvascular imaging and blood flow measurements by LSI approaches.

Label-free, noncontact, wide-field imaging of blood vessels with reasonable spatiotemporal resolution can be performed using speckle-based methods, which are distinguished for their instrumentational simplicity [24] with a strong potential for clinical use. However, it must be noted that unlike several other optical volumetric imaging approaches such as OCT, photoacoustic imaging, or TPM [18, 20, 37], LSI is primarily a surface-based imaging technique without depth discrimination, which must be kept in mind when interpreting images or choosing methods for particular biomedical applications.

Here, we evaluate various LSI approaches for blood flow measurement and classify them into three general categories based on their degree of quantification. Specifically,

1. **Qualitative**: LSI techniques that primarily visualize vessel morphology and offer some indirect blood flow information based on the speckle contrast analysis of the functional vascular network.
2. **Semi-quantitative**: LSI techniques that yield relative quantitative results, thus providing insight into the *spatiotemporal* distribution of metrics *proportional* to the blood flow based on simplified theoretical models.
3. **Quantitative**: LSI techniques that enable *absolute* quantitative measurements of blood flow *dynamics*, for example, providing the blood flow velocity field without any prior assumptions or scaling factors.

List of acronyms used in the article.

Name	Acronym	Name	Acronym
Dynamic light scattering imaging	DLSI	Red blood cell	RBC
Inverse correlation time	ICT	Rolling shutter speckle imaging	RSSI
Laser speckle contrast analysis	LASCA	Scientific complementary metal oxide–semiconductor	sCMOS
Laser speckle contrast imaging	LSCI	Sidestream dark field microscopy	SDF
Laser speckle imaging	LSI	Signal-to-noise ratio	SNR
Light-sheet laser speckle imaging	LSH-LSI	Spatial laser speckle contrast imaging	sLSCI
Multi-exposure speckle imaging	MESI	Temporal laser speckle contrast imaging	tLSCI
Optical coherence tomography	OCT	Transmission-detected LSCI	TR-LSCI
Optical speckle image velocimetry	OSIV	Two-photon microscopy	TPM
Particle image velocimetry	PIV	Region of interest	ROIs

TABLE 1 Comparison of laser speckle imaging (LSI) and other optical blood flow measurement modalities.

Imaging modality	Merits	Limitations
LSI [24, 25]	Noninvasive, high temporal resolution, provides 2D maps of blood flow, relatively simple	Limited depth penetration, sensitive to motion artifacts
Doppler-OCT [26–28]	High resolution, can image microvasculature, provides depth-resolved measurements	Limited field-of-view, relatively complex and expensive, sensitive to motion artifacts
Laser Doppler velocimetry [29, 30]	Noncontact, able to measure velocity and flow rates, useful in fluid dynamics	Limited to measuring flow in one point or very small area, sensitive to external disturbances
Multiphoton microscopy [31, 32]	High spatial resolution, enhanced imaging depth, reduced photodamage (compared to conventional microscopy)	Requires expensive equipment, complex, slower imaging speed
Diffuse correlation spectroscopy [33]	Noninvasive, can measure deep tissue blood flow, useful for monitoring cerebral blood flow	Lower spatial resolution, requires complex data analysis, sensitive to motion artifacts

Abbreviation: OCT, optical coherence tomography.

Figure 1 overviews the historical timeline of these categories with important methodologies that have shaped the LSI field. LSI began as a qualitative approach in 1981, evolved into semi-quantitative techniques after 2005, and has only recently become a quantitative technique, with each step providing further insightful information on the dynamics of tissue blood flow.

In this review, we begin by outlining the fundamentals of speckle physics with a focus on LSI implementations. We then provide a detailed description of each of the three categories, with illustrative instances of relevant results and enabling technologies and an overview of their applications. In light of recent developments and contemporary clinical demands, we conclude by exploring future directions for the advancement of LSI.

2 | SPECKLE BASICS RELEVANT TO LSI

When coherent light interacts with a scattering medium such as living biological tissue, a grainy texture known as a speckle pattern is observed in the resultant optical images. This pattern, and its spatial variation and temporal dynamics, carries important biophysical tissue information. The spatiotemporal variation of amplitude and phase of the detected speckle field arises from:

1. Interference of multiple-scattered light reflected off from the surface and subsurface tissue structures, including mobile scatterers (rotating, diffusing, convectively flowing, or otherwise moving over time in and out of given imaged locations).
2. Microscopic roughness of the imaged tissue surface.
3. Noise sources in the measurement system (e.g., electrical shot noise in the photodetector).

Besides photodetector noise, these factors contribute to a "random walk" in the phase and amplitude of scattered light interfering on the photodetector. The resultant electric field at a given location in space and time can be described by the mathematical construct of phasors [44]

$$A = \frac{1}{\sqrt{N}} \sum_{n=1}^{N} a_n e^{j\phi_n},$$

$$\mathcal{R} = \text{Re}\{A\} = \frac{1}{\sqrt{N}} \sum_{n=1}^{N} a_n \cos\phi_n; \mathcal{I} = \text{Im}\{A\}$$

$$= \frac{1}{\sqrt{N}} \sum_{n=1}^{N} a_n \sin\phi_n, \tag{1}$$

where A is the electric field phasor (a complex number), a_n and ϕ_n are its nth light amplitude and phase components with N being the total number of considered light phasors, and $\text{Re}\{A\}$ and $\text{Im}\{A\}$ are the real and imaginary parts of the total phasor. Most random walks satisfy the assumptions that a_n and ϕ_n are independent of each other. The square of the resultant electric field is the intensity of the speckle image.

For the fully developed speckle statistics, the probability density function for amplitude (a_n in Equation 1) follows the Rayleigh distribution and the phase ϕ_n is uniformly distributed [44, 45]. These conditions can be achieved by selecting a suitable laser for illumination along with a large number of random phasors detected on a sensitive imaging detector. For most speckle imaging techniques, such a fully developed speckle is a prerequisite. This is because LSI leverages the dependence of speckle on the motility of tissue scatterers to enable their differentiation (e.g., blood vessel pixels
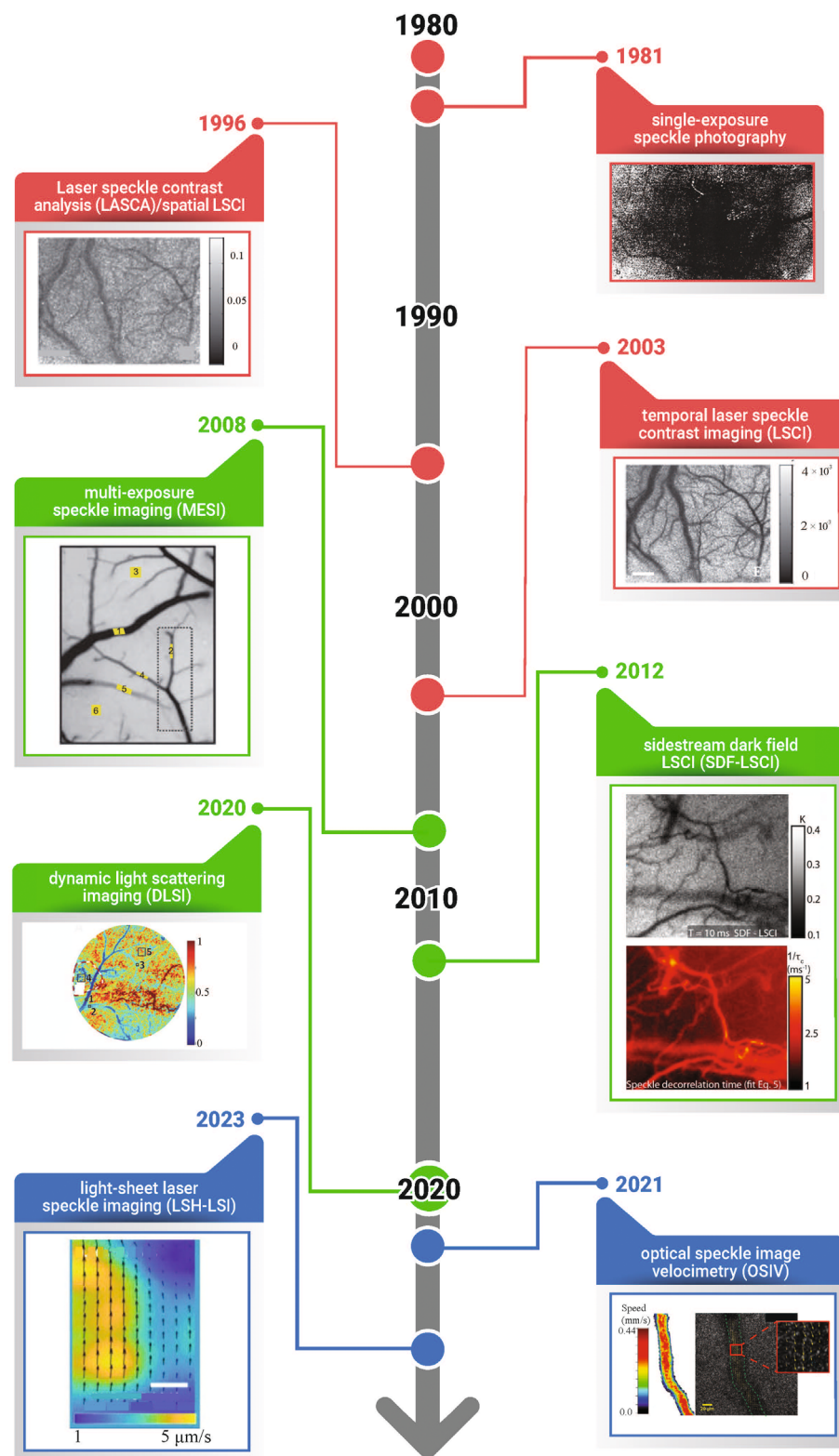
FIGURE 1 Evolution of laser speckle imaging (LSI) from qualitative to fully quantitative functional vascular flow imaging. The three different LSI categories summarized in this review are classified as qualitative (red), semi-quantitative (green), and quantitative (blue), as the static microvascular maps are increasingly supplemented with dynamic blood flow information. The representative images were all acquired in small rodent cranial window models, except single-exposure speckle photography, which was performed on a human retina and light-sheet laser speckle imaging (LSH-LSI) was performed on motile cilia organelle. Note that with time and technological advances, the resolution, processed image quality, and blood flow information reporting of LSI improves. *Source*: Adapted from Refs. [38–43] with permission.

containing RBC scatterers are characterized by shorter speckle decorrelation times than the pixels containing the relatively static surrounding tissue). Erroneous information about these underlying biophysical dynamics may result from underdeveloped speckle statistics, for instance, when measured decorrelation results from scatterer motion are contaminated by instrumental artifacts (e.g., insufficient acquisition rates resulting in undersampling). After achieving experimentally desirable, fully developed speckle pattern conditions, it is necessary to take into account various parameters and important experimental variables for all speckle

imaging. These include speckle contrast, speckle size, camera settings, and polarization analyzer as now described.

Arguably, the most common LSI-relevant parameter is the *speckle contrast*. It is a measure of how strong the *intensity variations* are compared to the *average intensity* of the speckled image. Spatial or temporal speckle contrast K is defined as the ratio of standard deviation σ to the mean intensity $\langle I \rangle$ of the speckled image [38]:

$$K = \frac{\sigma}{\langle I \rangle}. \qquad (2)$$

For a fully developed speckle, the theoretical maximum K value is unity. Importantly, speckle contrast is used to quantify the dynamic blurring of speckle patterns recorded by the camera with finite exposure time. When well-controlled/accounted for bulk tissue motion, the "solid" tissues are relatively static and can yield higher speckle contrast values with little blurring. Conversely, the speckle contrast caused by moving scatters (e.g., flowing RBCs inside vessels) decreases due to the smearing effect of speckle changes. Therefore, the speckle contrast is inversely proportional to the scatterer's motion, in this case blood flow.

Depending on the particular technological implementation, speckle contrast can be computed spatially or temporally by considering spatial (σ_s) or temporal (σ_t) standard deviations in the signal intensity. Generally, the spatial contrast has a poor spatial resolution (due to the size of the spatial averaging window used in its calculation) and higher temporal resolution (ability to distinguish changes in a dynamic process over time); conversely, the temporal speckle contrast has high spatial resolution but poor temporal resolution due to the temporal averaging over the stack of speckle images.

Speckle size is another important parameter to consider. All LSI setups use lenses and a camera detector, and the speckle size over the pixels of the detection sensor is described [25] as

$$S_{\text{speckle}} = 2.44\lambda(1+M)f\#, \qquad (3)$$

where M is the magnification of the optical system and $f\#$ is its f-number (the ratio of focal length to aperture diameter). In a typical optical system, laser wavelength and magnification are often constant, and therefore speckle size can be controlled/optimized by changing the $f\#$ (lens diameter and working distance). Speckle size in terms of camera pixels should be chosen wisely, as these pixels' intensity and standard deviation will determine the speckle contrast. In fact, Kirkpatrick et al. [46] argue that the optimal speckle size should be twice the camera's

pixel size to fulfill the Nyquist sampling principle, and indeed most reported LSI studies followed this criterion. If one does not have information about the optical system parameters, another way of estimating the speckle size is to compute the full width at half maximum of the power spectral density of the speckle pattern. The power spectral density and intensity autocorrelation function are a Fourier transform pair according to the Wiener–Khinchin theorem [47].

Several practical and important experimental variables require careful consideration in a typical LSI experiment. The exposure time of the imaging camera should be in a moderate range (typically between 1 and 30 ms) to ensure both reasonable speckle contrast and signal-to-noise ratio (SNR). Usually, the camera frame rate and exposure time are a reciprocal pair; however, in some techniques, the effective exposure time may vary independent of the camera frame rates (by optical gating of laser illumination, see multi-exposure speckle imaging [MESI] and optical speckle image velocimetry [OSIV] discussions in later sections) [43, 48]. In many LSI systems reported in the literature, a linear polarizer (analyzer) is commonly employed as an experimental design parameter in the imaging path between the camera and the sample to improve speckle contrast. This is especially useful because lasers are usually linearly polarized, and the orthogonally polarized analyzer helps minimize the direct surface reflection and extract more information regarding the interaction between light and the sub-surface tissue. The topic of speckle polarization is explored in greater detail in Ref. [49], where it is concluded that speckle contrast and signal information content can be maximized if the illumination and analyzer polarizations are perpendicular to each other.

LSI is dependent on experimental conditions, specifically: (i) laser wavelength that should match the optical properties of the tissue under investigation, (ii) selection of appropriate optics that influences the imaging resolution, and (iii) external environmental conditions, such as ambient light, vibrations, and temperature fluctuations that can introduce noise and artifacts in LSI measurements. Furthermore, the complexities arising from inherent tissue heterogeneity and the presence of inclusions such as bony structures or joints can also affect the speckle pattern and thus the quantification of blood flow. In comparison with the qualitative LSI techniques, the semi-quantitative techniques (MESI or dynamic light scattering imaging [DLSI]) can overcome these challenges and ensure reliable measurements even in complex tissue environments.

Typical LSI setups are shown in Figure 2. Commonly, the LSI measurement systems (Figure 2A) share the same configuration for the detection unit (focusing optics with an analyzer and an image sensor). For the illumination
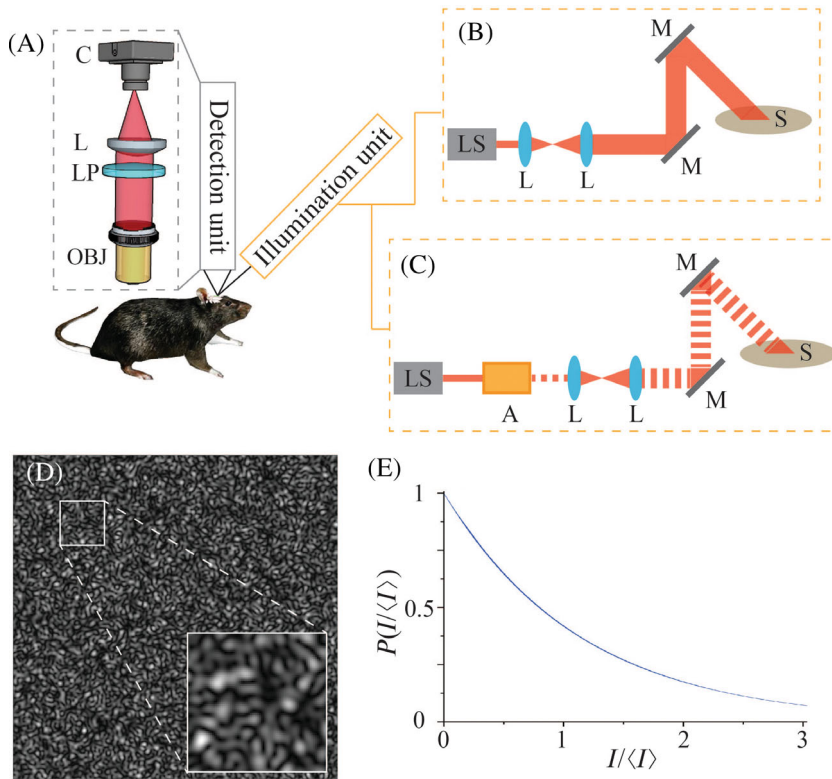
FIGURE 2 Typical laser speckle imaging (LSI) experiments and results. (A) Typical optical setup for the LSI, highlighting the illumination and detection units. The latter typically consists of collection optics (objective lens, tube lens), polarizer, and imaging sensor. (B) Common illumination setup for the LSI in which laser light is expanded and steered to illuminate the tissue sample. (C) Implementation of optical modulation/gating to reduce the smearing of fast-moving speckles and enable contrast and signal-to-noise ratio improvements. (D) Representative granular speckle pattern. (E) The negative-exponential probability density function for intensity is one of the statistical properties of fully developed speckle pattern shown in (D). A, acousto-optic modulator; C, imaging sensor; $I/\langle I \rangle$, intensity at a considered pixel normalized by its average; L, lens; LP, analyzer; LS, laser source; M, mirror; OBJ, objective lens; S, sample.

unit, a coherent light source such as a laser or laser diode along with the beam expander is required to illuminate the sample, typically at an oblique angle (Figure 2B). Examples of this type of setup include spatial laser speckle contrast imaging (sLSCI), temporal laser speckle contrast imaging (tLSCI), and DLSI. Some techniques, including MESI and OSIV, utilize optical gating to enhance contrast and SNR as well as better control over the camera exposure by use of an acousto-optic modulator, which works by diffracting the laser beam to gate the exposure (Figure 2C). In general, there are no major hardware differences between different types of LSI imagers. However, the way in which speckle images are acquired and processed after imaging can vary significantly, as discussed in more detail below. A raw speckle image (Figure 2D) with a negative-exponential probability density function for intensity (Figure 2E) described by Rayleigh statistics, one of the statistical properties of the fully developed speckle pattern, is also shown. It is worth noting that owing to their relative technological simplicity, LSI techniques can be combined with other optical modalities, such as sidestream dark field microscopy-laser speckle contrast imaging (SDF-LSCI), to enable hybrid capabilities and integrate into existing microscopy systems.

After this brief primer on speckle physics and technology relevant to LSI, we now turn to the specific technological implementations and their associated results. We begin with qualitative techniques.

3 | TECHNIQUES WITH QUALITATIVE OUTPUT

The first laser speckle technique used to show the spatial map of tissue blood vessels was introduced in 1981 as single-exposure speckle photography [38] as shown in Figure 1. Subsequently, its application was demonstrated to produce maps of human retinal blood microvasculature [50, 51]. A relationship was established between camera exposure time and correlation function with the spatial speckle contrast through this technique. It involved a simple spatial filtering technique and yielded spatial variance (σ_s^2) of the time-averaged speckle pattern, which is equivalent to the integration of autocovariance over the camera exposure time (T):

$$\sigma_s^2(T) = \frac{1}{T} \int_0^T C(\tau)\, d\tau. \tag{4}$$

$C(\tau)$ is the autocovariance of the intensity defined as

$$C(\tau) = \left\langle \left(I(t) - \langle I \rangle_t\right)\left(I(t+\tau) - \langle I \rangle_t\right)\right\rangle, \tag{5}$$

where $\langle \cdots \rangle_t$ represents time averaging. For the quantification of time-averaged speckle fluctuation, electric field autocorrelation $g_1(\tau)$ can be used, but this can be challenging to measure. As an alternative, the intensity

autocorrelation $g_2(\tau)$ is commonly employed. The relationship between $g_1(\tau)$ and $g_2(\tau)$ is known as a Siegert relationship [52, 53]:

$$g_2(\tau) = 1 + \beta |g_1(\tau)|^2, \tag{6}$$

where β is the normalization factor here assumed to be 1. The covariance can be related to temporal intensity autocorrelation $g_2(\tau)$ for the quantification of time-averaged speckle fluctuation, with the assumption of a negative exponential dependence [54, 55]. The autocovariance:

$$C(\tau) = \langle I \rangle^2 |g_1(\tau)|^2. \tag{7}$$

From the normalized autocovariance and Siegert relationship, we can have the autocovariance as

$$C(\tau) = \langle I \rangle^2 \exp\left(-\frac{2\tau}{\tau_c}\right), \tag{8}$$

where τ_c represents the correlation time that characterizes the dynamics of the scatterers. When specific conditions are met, such as small scattering angles and single scattering, the correlation time is inversely proportioned to the mean velocity of the scatterers such as RBCs, $\tau_c \propto (1/v)$ [52]. Thus, in addition to spatial visualization of blood vessels, which was characteristic of early LSI studies, some indications of blood flow dynamics (albeit under strict assumptions/conditions) also began to emerge at this stage. The relationship between the spatial and temporal statistics of time-integrated speckles (i.e., spatial variance) can be derived by combining Equations (5) and (8).

$$\sigma_s^2(T) = \left(\frac{\langle I \rangle^2 \tau_c}{2T}\right)\left[1 - \exp\left(-\frac{2T}{\tau_c}\right)\right]. \tag{9}$$

From Equations (2) and (9), the local spatial speckle contrast becomes

$$K_s = \frac{\sigma_s}{\langle I \rangle} = \sqrt{\left(\frac{\tau_c}{2T}\right)\left[1 - \exp\left(-\frac{2T}{\tau_c}\right)\right]}. \tag{10}$$

Equation (10) above explains that the speckle contrast decreases if the speckle decorrelation time τ_c is smaller than the camera exposure time T. When there is movement of RBCs in the blood vessel, the speckle becomes blurred because the speckle decorrelates rapidly. Also, higher speckle contrast is observed if τ_c is bigger than T

for relatively static surrounding tissue. Therefore, a microvasculature map can be obtained with the relationship between speckle decorrelation time and speckle contrast.

With the advent of digital cameras, laser speckle contrast analysis [56, 57] was introduced so that spatial filtering can be directly performed within the digital camera's probing window. The size of the latter (in terms of pixels) is an important factor for computing local speckle contrast for the spatial resolution of the blood flow map, as per Equation (9). Generally, the window size for most spatial LSI is 5×5 or 7×7 pixels to get reasonable spatial resolution and sufficient pixel numbers for robust speckle statistics calculations (henceforth designated sLSCI). Most sLSCI studies were performed with the camera's global shutter setting. However, Du et al. [58] showcased the use of sLSCI with a rolling shutter setting, indicating that with the resultant line scan LSCI, the image contrast could be improved.

The sLSCI technique gives a qualitative microvascular map based on speckle contrast variation between the blood vessel containing moving RBCs and surrounding "static" tissue. This is an effective approach for imaging large vascular maps (like in cerebral ischemia [59] or cortical spreading depression [60]). The sLSCI technique has two drawbacks. Firstly, it has limited spatial resolution because the speckle contrast parametric map is calculated over the neighboring pixels (typically 5×5 or 7×7 pixels window). Secondly, the resulting vessel visualization provides little dynamic or flow information, as the relationship between the correlation time and velocity relationship $\tau_c \propto (1/v)$ is subject to strict assumptions.

An alternative approach to address sLSCI's spatial resolution limitation and improve the detection of slower-flowing blood vessels is to perform temporal processing of the raw speckle pattern [39,61,62]; in other words, one can calculate speckle contrast at the same pixel location over the time series of speckle images (tLSCI). Note that this is analogous to speckle-variance OCT, a widely used alternative method for volumetric subsurface imaging of the microvasculature [63-65]. To compute the temporal speckle contrast K_t, first- and second-order temporal statistics are invoked (pertaining to the average and variance, respectively) [39]. Equation (2) thus becomes

$$K_t = \frac{\sigma_{i,j}}{\langle I \rangle_{i,j}} = \frac{\sqrt{(1/(N-1))\left\{\sum_{n=1}^{N}\left[I_{i,j}(n) - \langle I_{i,j} \rangle\right]^2\right\}}}{\langle I \rangle_{i,j}}, \tag{11}$$

where (i,j) is the pixel location, N is the number of acquired images, $I_{i,j}(n)$ is the intensity at (i,j) pixel at nth image, and $\langle I_{i,j} \rangle$ is the mean intensity value at (i,j) for N images.

As discussed in the previous section, LSCI imaging is typically performed in reflection mode. Nevertheless, the first LSCI was carried out in transmission mode in mice [66], wherein the laser source was positioned underneath the tissue; recently, transmission-detected LSCI (TR-LSCI) has been applied to qualitatively monitor blood flow in thick tissues including the human hand (finger and opisthenar of a young, healthy volunteer) [67]. LSCI is compatible with other in vivo applications including micro/compact endoscopy [68,69], hyperspectral imaging [70], microscopic [71], and intraoperative surgery [72-74]. LSCI can also be integrated with fluorescent intravital microscopy, enabling the estimation of perfusion rates and differentiation of arteries from veins in the mouse brain [75,76].

Figure 3 compares different qualitative LSI techniques to visualize tissue microvascular patterns. Compared to sLSCI, tLSCI provides better spatial resolution and contrast and allows for the visualization of slower-flowing fine microvessels (Figure 3A). However, this temporal processing requires repeated imaging of the same location (25 frames in the example shown); this makes tLSCI slower and degrades its temporal resolution (e.g., compromising its ability to detect fast physiological processes). In contrast to tLSCI, sLSCI acquires a single frame and, while it may miss some slower-flowing vessels resulting in a less sharp vessel visualization map, it offers a higher temporal resolution (potentially important is negating tissue motion artifacts and monitoring fast physiological processes). Figure 3B compares conventional reflection-mode LSCI with TR-LSCI in different mouse organs, with the latter showing somewhat improved spatial resolution. However, note that TR-LSCI can perform qualitative imaging to maximum tissue thicknesses of ~3–5 mm but cannot distinguish the depth of vessels, so its range of clinical applications is limited and reflection-mode LSCI may prove more practical.

Significant efforts to improve these qualitative speckle imaging techniques include noise reduction [77,78], characterization of the relationship between speckle contrast and the camera's pixel size [46], spatial resolution improvements without sacrificing temporal resolution (by introducing an external rotating diffuser that creates random speckle field over the sample) [79], motion correction [80], depth of field improvement [81], and data processing pipeline development for real-time microvascular tree visualization [82].

For retina blood flow, LSI is referred to as laser speckle flowgraphy. The mathematical formulas and terms used for estimating the blurring of speckles caused
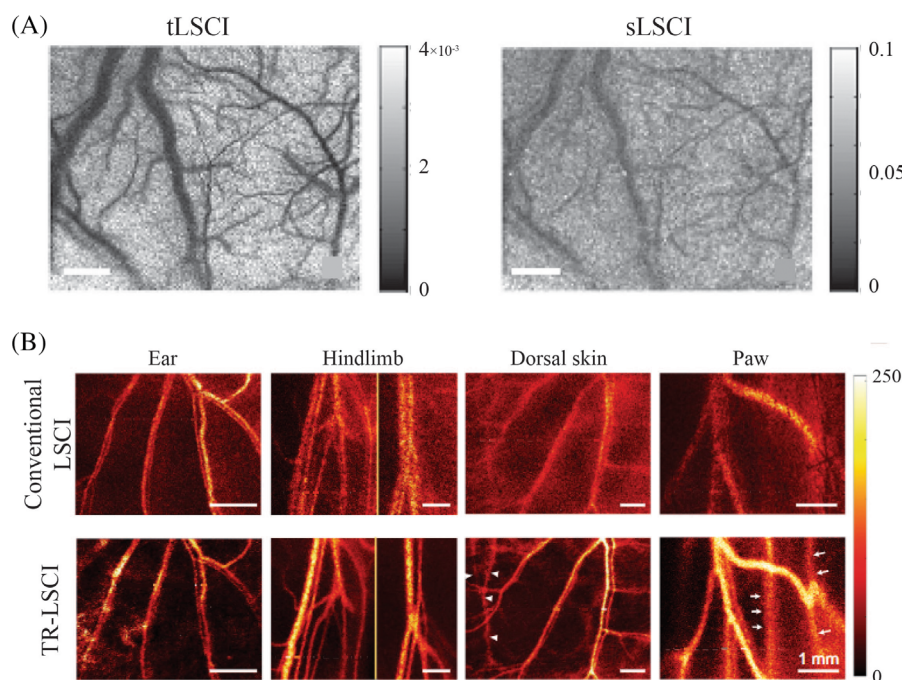

FIGURE 3 Comparison of qualitative laser speckle imaging techniques. (A) Temporal and spatial laser speckle contrast imaging (LSCI) in the rodent brain. Temporal laser speckle contrast imaging (tLSCI) used 25 frames of speckle images, while spatial laser speckle contrast imaging (sLSCI) used a single speckle image; tLSCI thus has a better spatial resolution (and improved contrast) while sLSCI has superior temporal resolution (for details, see text). The gray-scale bars indicate the speckle contrast value ranges. Scale bars: 500 μm. (B) Improvements enabled by transmission mode relative to conventional reflection mode LSCI in various mouse organs. Color bar indicates the speckle contrast values range. TR-LSCI, transmission-detected LSCI. *Source*: Adapted from Refs. [39,67] with permission.

by microcirculation in the retina are slightly different and are summarized in another recent review paper [83]. Qualitative LSI methods, including laser speckle flowgraphy, have been widely adopted and proven to be effective in various clinical settings; examples of LSI imaging at different human sites are shown in Figure 4. Further similar human investigations and future clinical trials deploying related LSI approaches are also anticipated. However, a major limitation of qualitative LSI is the relative lack of quantitative dynamical blood flow information.

It is worth re-emphasizing that all of these LSI techniques for visualizing tissue blood vessels are noninvasive, contrast-agent-free imaging methods with widefield imaging capabilities and simple optical setups. They can also be integrated with other modalities and post-processing algorithms to produce excellent qualitative images of tissue microvasculature. Table 2 shows various LSI techniques' (qualitative and beyond) preclinical and clinical applications with features, limitations, and their integration with other instrumentation.

4 | TECHNIQUES WITH SEMI-QUANTITATIVE OUTPUT

While qualitative techniques are commonly used clinically, they yield speckle contrast that primarily enables visualization of the microvascular tree structure. While this imaging of the vessel architecture is important and useful, the information about the blood flow dynamics in these detected vessels is limited. Furthermore, these
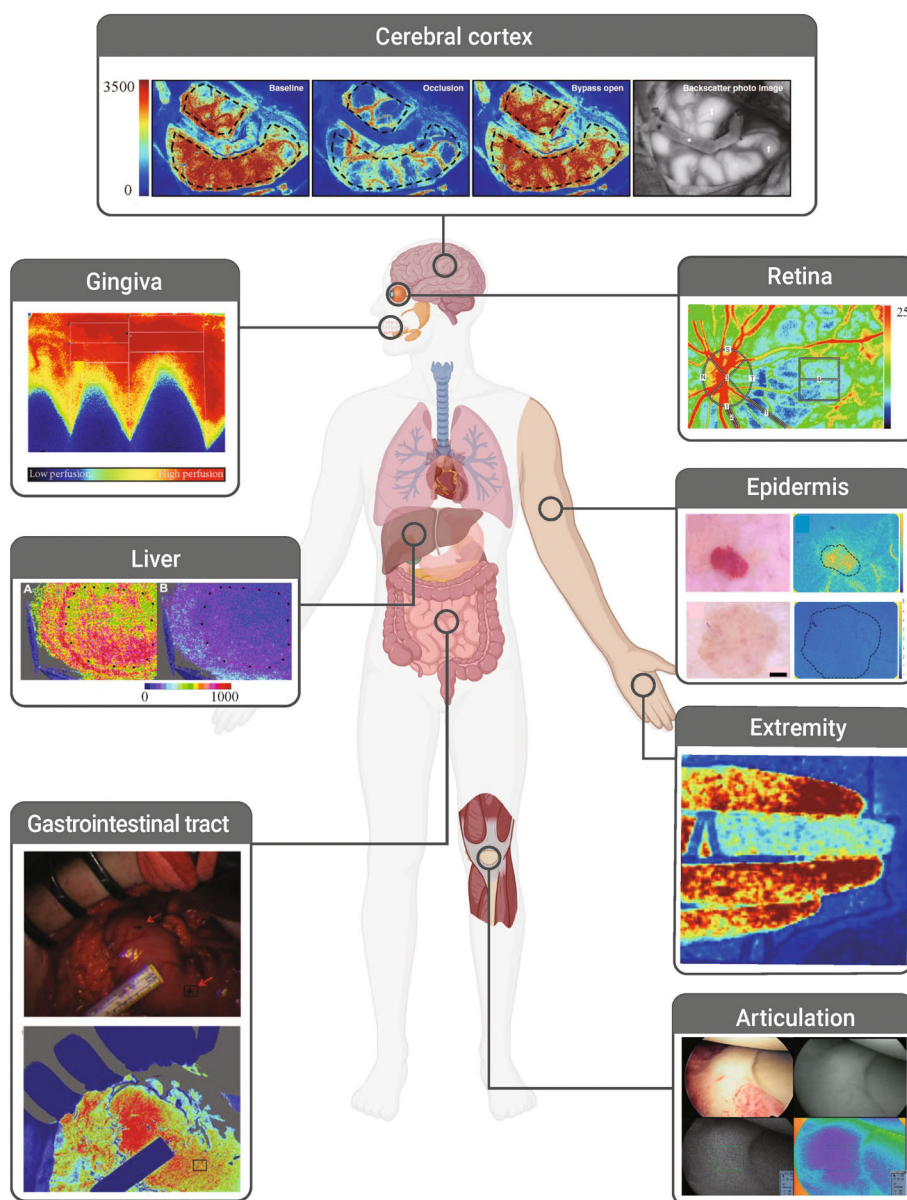

FIGURE 4 Clinical applications of laser speckle imaging (LSI). Beyond preclinical imaging, LSI has been widely employed in various human studies. Illustrative examples range from noninvasive superficial imaging of the human retina [84], gingiva [85], epidermis [86], and extremity [87] to minimally invasive endoscopic and intra-operative imaging of the cerebral cortex [88], liver [73], gastrointestinal tract [89], and articulation [90].

TABLE 2 Laser speckle imaging (LSI) preclinical and clinical applications.

Application	Technique	Features	Limitations
Retinal blood flow imaging	Single-exposure speckle photography [50, 51]	Can differentiate between tissue and vessels with an analog camera and filter Noninvasive	Requires manual post-processing on the photograph of analog camera Poor spatial resolution
	Laser speckle flowgraphy [84,91-93]	Improved spatial resolution (can observe retinal microvasculature) Use of normalized blur instead of speckle contrast to show speckle fluctuation Noninvasive	Calibration is required for all the ROIs (even within a single eye)
	sLSCI/tLSCI (laser speckle flowmetry) [94,95]	Enables retinal blood flow monitoring without stimulating retinal neurons Enables measurement of blood flow in choroidal vessels of the eye Noninvasive	Only offers qualitative visualization of low/high blood flow
Microvascular endothelial function	LSCI [96,97]	Measure the relationship between cardiac disease and endothelium-dependent skin microvasculature Real-time and noninvasive measurement of cutaneous microvascular perfusion changes	Single time-point measurements (no 2D microvascular maps are generated)
Skin disease diagnosis and progression monitoring	sLSCI and tLSCI [86,98-102]	Enables assessment of skin microvasculature for pathological change in blood flow Accelerates initial assessment of disease Noninvasive	Only offers qualitative visualization of low/high blood flow
Cerebral blood flow monitoring for surgical guidance (e.g., extracranial–intracranial bypass, cerebral aneurysm clipping, carotid endarterectomy)	sLSCI and tLSCI [72,103-106]	Enables real-time monitoring of functional activity of the brain (cerebral blood flow) during surgery Direct intraoperative microscopy integration	Low spatial resolution (minimally) invasive during intraoperative procedures
Oral health monitoring toward early detection of tooth decay	sLSCI [107-109]	Ease-of-use by dental practitioners for noninvasive analysis of extracted teeth Improved contrast for tooth decay (beyond white-light illumination)	Most tooth decay studies performed *ex-vivo* Qualitative nature of decay assessment
Laparoscopy for disease diagnosis and assessment of tissue functional status (various organs)	MESI [110]	Reasonable flow estimation with speckle variance and camera's exposure time graphs Direct intraoperative microscopy integration	No human studies, mostly small animal imaging to date (minimally) invasive during laparoscopy

Abbreviations: LSCI, laser speckle contrast imaging; MESI, multi-exposure speckle imaging; sLSCI, spatial laser speckle contrast imaging; tLSCI, temporal laser speckle contrast imaging.

methods are incapable of estimating the effect of static scattering (stationary speckles) on the speckle contrast in the dynamic regions of interest (e.g., thin tissue or fat layer covering blood vessels), leading to inaccurate spatiotemporal parameters. Indeed, in the presence of an overlying static layer (common in many clinical scenarios), the variations in the scattered field follow a Gaussian distribution, but the measured signal gains an additional static component that causes the resultant intensity to deviate from Gaussian statistics [44]; consequently, the Siegert relation in Equation (6) cannot be utilized.

MESI was introduced to enable more quantitative analysis of flow dynamics and overcome the static layer limitation [48]. In MESI, multiple speckle images are taken with different exposure times (ranging from 50 μs to 80 ms), and the resultant combination generates a single MESI image. Experimentally, optical gating (multiple exposure times) is achieved with the help of an acousto-optic modulator (AOM) and a pulse generator (Figure 2C), while the camera frame rate and exposure time remain constant. The speckle variance curve was computed for each exposure time to determine the decay rates (thus yielding the autocorrelation function curve and relative decorrelation time) to estimate flow rates/velocity ($\tau_c \propto (1/v)$). The speckle contrast in MESI was derived as

$$K(T, \tau_c) = \sqrt{\beta \rho^2 \frac{e^{-2x} - 1 + 2x}{2x^2} + 4\beta \rho (1 - \rho) \frac{e^{-x} - 1 + x}{x^2} + v_s},$$

(12)

where $\rho = I_d/(I_d + I_s)$ is the fraction of dynamic light scattered with I_d and I_s being the dynamic and static scattered light intensities, respectively. $x = T/\tau_c$ and $v_s = v_{noise} + v_{ne}$ is the sum of the variance of experimental noise (v_{noise}) and ambient/background light (v_{ne}). In MESI (unlike in LSCI), β is not assumed equal to 1. MESI accounts for the presence of the static scattering overlayer by introducing ρ in its governing Equation (12), while v_{noise} and v_{ne} terms help improve the technique's resolution and contrast. The blood flow map for MESI is shown as a parametric image of inverse correlation time (ICT) with the unit of (s^{-1}). Figure 5A demonstrates a typical example based on eight frames of different exposure times. Also shown is the dependence of temporal speckle variance on the camera exposure time for different ROIs in MESI output. Using Equation (12), each curve is fitted for ROIs in MESI output. The exponential decay of red curves for the tissue ROIs is slower than the blue curves for those representing blood vessels.

In comparison with LSCI, the clinical applications of MESI have been limited to date [112]. However, in preclinical research, MESI is widely used for studies of cortical blood flow [40], vasodilation [113], and laparoscopy [110]. The primary constraint of this technique is its inadequate temporal resolution caused by inter-frame dead time, which stems from the need for multiple images captured at varying exposure times. To address this limitation, single-photon avalanche diode arrays were utilized [114] with high acquisition rates and single-photon sensitivity.

A novel approach called DLSI [42] has been introduced to enhance temporal resolution. By employing a high-speed camera (with a frame rate of ∼20 000 fps), it measures temporal intensity autocorrelation $g_2(\tau)$ at every pixel. DLSI measures the correlation time accurately and properly accounts for static overlayer contribution (better than LSCI or MESI), its fitting model drawing on the known biophysical properties of RBCs (type of motion, scattering regime, and noise effects) and static scattering information. The intensity autocorrelation $g_2(\tau)$ was defined as [38]:

$$g_2(\tau) = \frac{\langle I(t) \times I(t+\tau) \rangle}{\langle I(t) \rangle \langle I(t+\tau) \rangle}$$

(13)

and $g_1(\tau)$ as

$$g_1(\tau) = \exp\left(-\left(\frac{\tau}{\tau_c}\right)^n\right).$$

(14)

In contrast to most speckle imaging models that assume $n = 1$, representing single scattering from RBCs, DLSI considers the value of n that depends on the presence of single or multiple scattering, and the type of motion such as RBC flowing or Brownian motion. DLSI also adjusts the β parameter in Equation (12) depending on the temporal and spatial averaging of the speckle pattern. DLSI thus represents a promising new technique with significant fundamental improvement in the LSI family, such as yielding interesting results for the relative blood flow index. DLSI with LSCI is compared in Figure 5B along with the dynamic light scattering regime maps for normal and ischemic conditions.

Another novel LSI implementation called rolling shutter speckle imaging (RSSI) was recently introduced [111]. RSSI utilizes a single frame of a rolling shutter camera to compute the row-by-row intensity correlations for 30 × 30 pixels window size and form an intensity correlation difference map $\Delta g_r(\tau)$ with a sliding window approach; a theoretical model to quantify the autocorrelation time (τ_c) is then utilized and the resultant correlation difference map, averaged autocorrelation time,
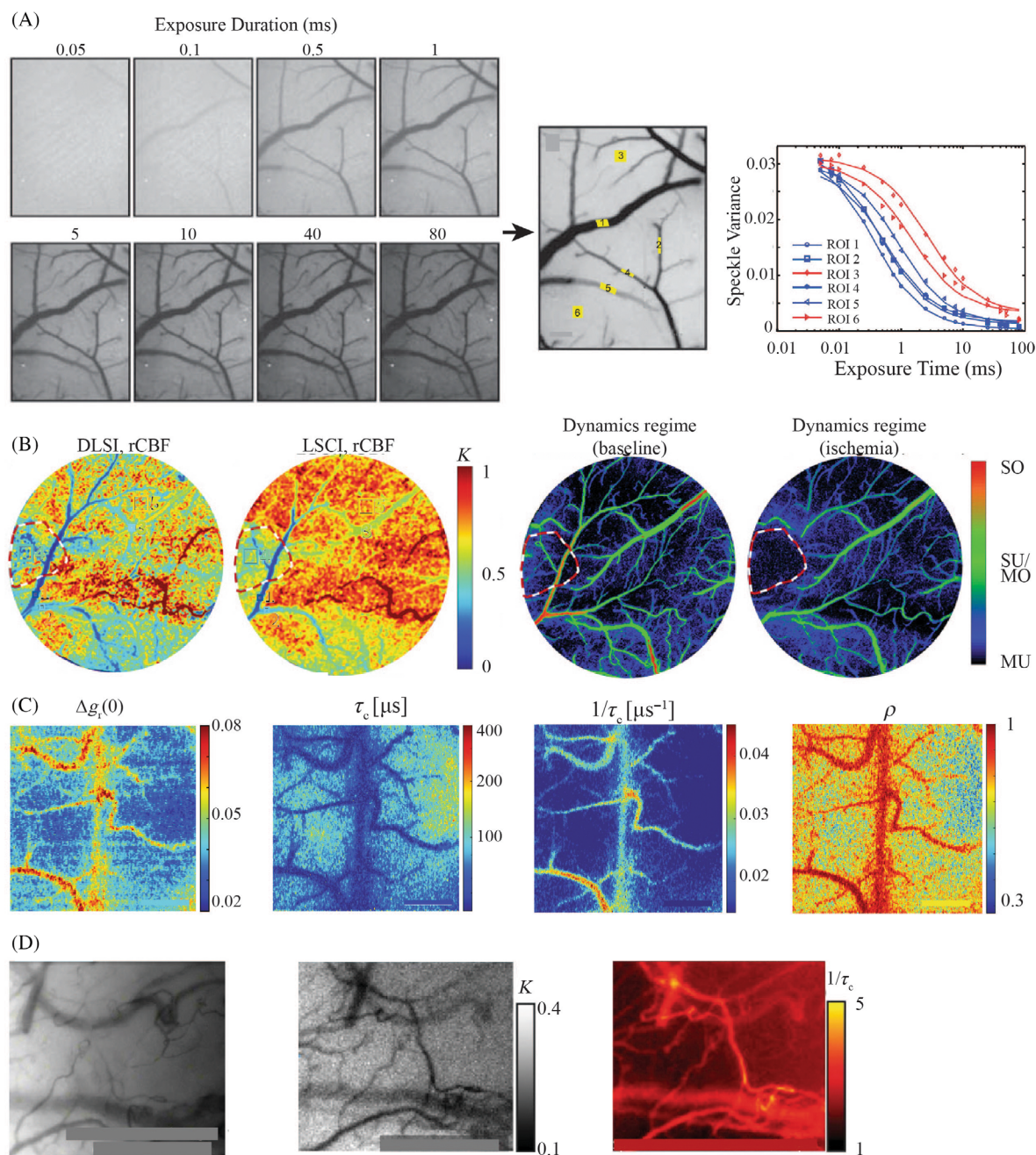
FIGURE 5   Blood flow estimation with semi-quantitative laser speckle imaging techniques. (A) Multi-exposure speckle imaging (MESI) principle combines multiple single-exposure images (right panels, left of figure) into a MESI output (middle); plots of the speckle variance versus exposure time at different ROIs in the middle MESI image (right). The red curves are for the ROIs of static tissue while the blue curves are for the blood vessel ROIs. (B) Comparison of relative cerebral blood flow index (rCBF) measured by dynamic light scattering imaging (DLSI) and laser speckle contrast imaging (LSCI) technique (color bar represents the speckle contrast values). Also shown on the right are the dynamic light scattering regimes mapped for normal and ischemic conditions, based on a priori knowledge of the scattering properties and motility of the RBC scatterers. The color bar represents the scattering regime and motion type (SO: single-ordered; SU: single-unordered; MO: multiple-ordered; MU: multiple-unordered). (C) Output of the RSSI technique with a correlation difference map $\Delta g_r(0)$ that shows the relative blood flow information, which is the basis of this model, followed by the averaged decorrelation, inverse decorrelation, and static layer (ρ) maps. (D) Output of a single sidestream dark field microscopy (SDF) acquisition and the qualitative LSCI (SDF-LSCI), showing (from left to right) a representative acquisition of conventional SDF, an output of SDF-LSCI, and a map of inverse correlation time from multiple acquisitions. *Source*: Adapted from Refs. [40-42,111] with permission.

inverse autocorrelation time, and static layer maps are shown in Figure 5C. Despite this abundance of obtainable novel information, RSSI has relatively poor spatial resolution when the speckle fluctuations are slow (e.g., capillary flow, Brownian motion in stagnant vessels). In summary, it is worth noting the new information that LSI is now able to provide regarding microvascular flow dynamics, goes beyond the microstructural vessel maps that were previously available (i.e., qualitative methods and Figure 3).

Another recent innovation by Nadort et al. is a technique named SDF-LSCI [41,115] that combines SDF [116] with LSCI to further drive LSI toward quantitative analysis. The optical setup for the system consists of a modified SDF system (illumination with broadband green light) by the coupling of red laser light for LSCI. The authors note that the decorrelation time was measured more accurately by acquiring the speckle images with multiple exposure times (Figure 5D). The SDF-LSCI technique is based on the theoretical model describing the optical and scattering properties of RBCs under the assumption that the scattering properties of RBCs in the microvasculature are constant. The assumption simplifies the rescaling factor for multiple scattering that can be used in the fitting model based on the Mie–Percus–Yevick scattering model [117]. The scaling factor for multiple scattering relies heavily on the model used, as the Lorentzian and Gaussian model assumptions lead to an underestimation or overestimation of velocity, respectively [115,118].

Figure 5 shows the representative results of the four techniques discussed in the semi-quantitative LSI category (a) MESI, (b) DLSI, (c) RSSI, and (d) SDF-LSCI outputs. Overall, it is clear that all semi-quantitative LSI techniques discussed here are more informative of blood flow dynamics compared to the qualitative techniques. Additionally, LSI techniques in this category properly account for the presence of the static tissue overlayer. For instance, MESI offers speckle variance and exposure time plots, DLSI includes a blood vessel map based on the type of RBC motion, and RSSI features average decorrelation time plots from which blood speed can be estimated. However, the main shortcoming of all semi-quantitative techniques remains their dependence on biophysical models of unknown validity.

5 | TECHNIQUES WITH QUANTITATIVE OUTPUT

Semi-quantitative techniques have an advantage over qualitative techniques by providing more detailed information on blood flow dynamics. Nevertheless, their implementation can be challenging due to their reliance on certain assumptions, incorporation of theoretical models, and adherence to strict conditions. This can make it difficult to utilize them in longitudinal studies where some of the physiological parameters likely change over time. A novel speckle imaging method named OSIV was devised to enhance the accuracy and precision of blood flow velocity and direction measurement [43]. Note that while most of the other LSI formulations have a common theoretical basis (like the relationship between the extent of speckle blurring and RBCs' motion), OSIV is inspired by another approach called particle image velocimetry (PIV) in fluid mechanics [119,120] that relies on the translation of speckles.

In OSIV, a time series of speckle images is taken and a temporal cross-correlation is performed on consecutive images over the small spatial region (probing window). In the experimental setup, an AOM was used for gating the illumination light, enabling rapid speckle imaging by reducing the effective exposure time of the scientific complementary metal oxide–semiconductor (sCMOS) sensor. OSIV can measure RBC speed up to 7 mm/s, with the maximum detectable speed limited by the camera frame rate (∼200 fps). Figure 6A–F shows OSIV applied to different stages of photothrombotic stroke in a mouse model, and the blood flow is measured in absolute units of (mm/s) along with flow direction.

The OSIV technique relies upon the translation of speckles, necessitating a fast camera and additional AOM to ensure the minimum exposure time is maintained. Furthermore, the output velocity map of OSIV fails to depict small vessels (limitation of detecting slow flows) and does not address the problem of the static layer overlying the vessels. Therefore, additional improvements are required to fine-tune and optimize this promising technique for evaluating blood flow.

Inverted light-sheet microscopy [122] was combined with LSI to create another approach capable of providing absolute numerical values associated with biophysical motion dynamics merged. Known as light-sheet laser speckle imaging (LSH-LSI) [121], it employed the principle of OSIV and PIV to measure velocities in vitro, such as ciliary beating frequency and the direction of cilia motion in different phases of motile cilia [123] in a Petri dish. A spatial averaging window size of 8×8 pixels was utilized, and the temporal cross-correlation was calculated using PIV software integrated into MATLAB (MathWorks, MA, USA) [124]. Figure 6G–J displays the raw speckle image obtained with LSH-LSI for the spatial pattern of ciliary beating, along with the corresponding quantitative velocity maps for the different conditions (power stroke and recovery stroke) of motile cilia in a Petri dish. The primary drawback of this light-sheet technique is that the optical setup utilizes transmission light-sheet geometry, which
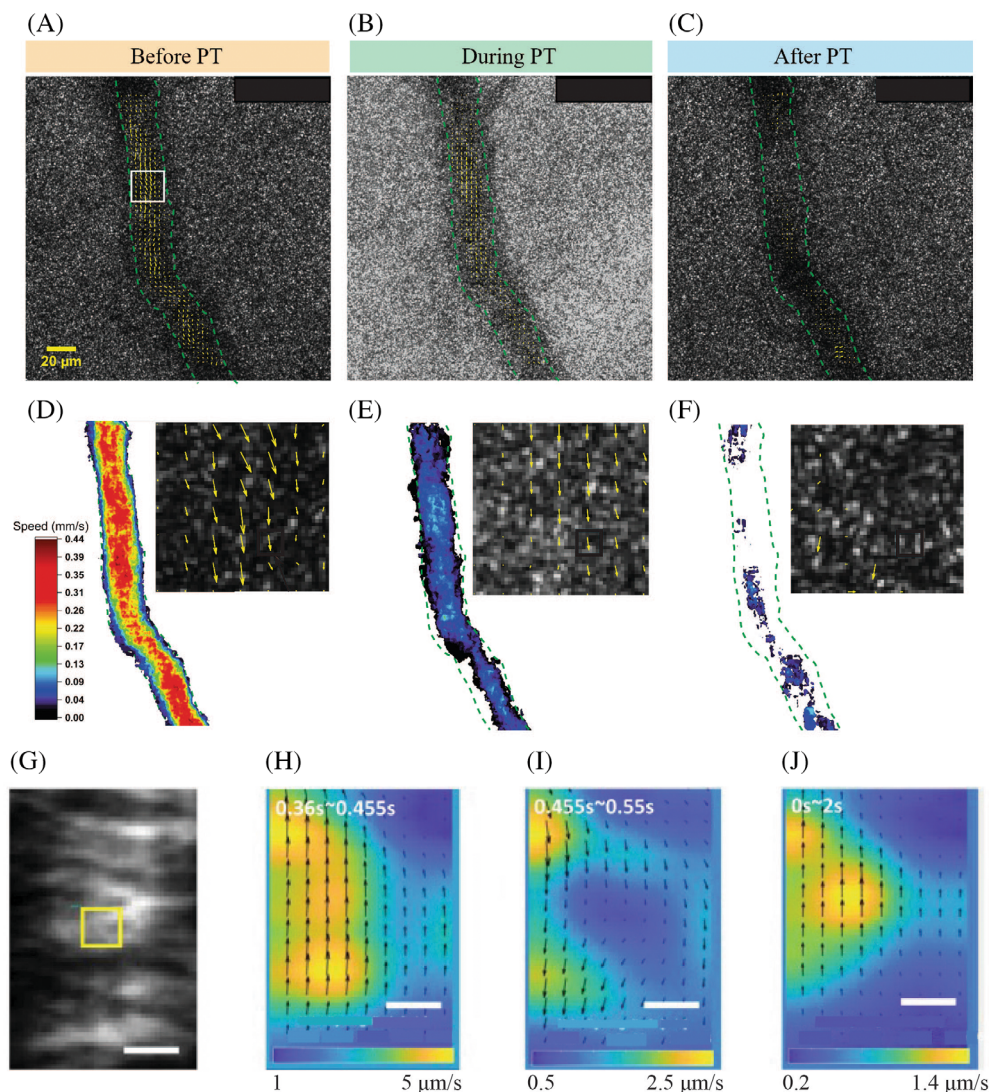
FIGURE 6 Blood flow dynamics with quantitative LSI. (A–C) Optical speckle image velocimetry (OSIV) map overlayed on the raw speckle images for the three stroke conditions (pre-, during-, and post-) in a cranial window mouse model. The field of view is 164×164 μm [2]. (D–F) Magnitude (colormap of the vessel) and direction (yellow arrows in the insets) of the velocity vector in the three stages of stroke. The magnified flow vector map of the boxed region in (A) is shown in each panel. OSIV can thus observe and quantify the blood flow changes during the three stages of strokes. (G) Raw speckle image from the light-sheet laser speckle imaging along with the interrogation window (yellow square box) of 8×8 pixels of motile cilia in a Petri dish. (H–J) The derived velocity maps (speed with colormap and direction with arrows) of the ciliary beat spatial pattern for the power stroke (H), recovery stroke (I), and velocity map for 2 s (J). Scale bar: 2 μm. PT, photothrombosis stroke. *Source*: Adapted from Refs. [43,121] with permission.

limits its application to in vitro or thin samples and renders it unsuitable for thick in vivo tissues.

Quantitative speckle imaging methods including OSIV and LSH-LSI are especially useful for longitudinal studies as they do not rely on calibration or any prior assumptions/information about the tissue. Furthermore, the velocity maps obtained from these techniques offer insights into both the magnitude and direction of RBC motions as they are based on speckle translation rather than speckle contrast and fluctuation like the techniques in previous categories. Despite their advantages,

quantitative techniques (Figure 6) are currently restricted to providing averaged velocity and a relatively limited field-of-view. Efforts are underway to enhance the slow-flow detectivity and wide-field imaging capabilities of these newly developed fully quantitative LSI methods.

6 | DISCUSSION AND OUTLOOK

The intricate details of hemodynamics play a pivotal role in determining the overall tissue status, enabling early

disease detection, diagnosis, treatment selection, and response monitoring, as well as the assessment of drug safety and efficacy. In this regard, LSI was developed in the 1980s for imaging and monitoring the blood vasculature, including the architecture of the microvascular tree and the dynamics of blood flow within it. LSI provides several benefits in terms of technical and systematic advantages. These include a wide field of view, label-free contrast based on speckle physics, a noncontact nature, and relatively simple instrumentation. In addition, LSI can provide valuable biophysical information about the tissues being studied, which may have important clinical implications.

The ergodicity assumption in LSI implies that the temporal and spatial speckle contrasts are interchangeable. However, this may not hold true in certain situations, such as low blood flow or insufficient exposure time, where the changing dynamics of the speckle pattern may not be adequately captured. This violates the ergodicity assumption and can lead to inaccuracies in visualizing or estimating blood flow [44,125]. Semi-quantitative techniques such as MESI and DLSI have been proposed to overcome this limitation. MESI, for instance, shows promise in addressing the challenge of non-ergodicity by capturing speckle images at different exposure times, thus accounting for the varying dynamics of the speckle patterns [40,48]. Moreover, the emergence of deep learning approaches also presents a novel avenue to tackle this issue; for example, recent research has demonstrated the effectiveness of machine learning algorithms in mitigating non-ergodicity, with a promise of more accurate blood flow measurements [126].

The biological zero problem in LSI refers to the challenge of accurately determining the speckle contrast baseline or "zero-flow" state in biological tissues. This baseline is crucial for quantifying relative changes in blood flow or other dynamic processes. However, biological tissues exhibit inherent scattering and microvascular activity even under baseline conditions, leading to a non-zero speckle contrast that can confound flow measurements [127]. The magnitude of the biological zero problem can be substantial, as it affects the baseline measurement and can lead to the overestimation of blood flow. This is particularly crucial in studies where small changes in flow are to be detected, or when comparing flows between different tissues or individuals. To address this, some studies have employed a subtraction method, whereby the biological zero state is measured separately in a zero-flow condition, and this value is then subtracted from the actual measurements. However, this method has inherent limitations as the baseline can vary between individuals and tissues, and over time [127,128]. Another way to deal with the biological zero is to integrate LSI

with other modalities (e.g., fluorescence imaging [129]) to provide complementary information that overcomes the associated limitations.

LSI has made significant progress in the past few decades, moving toward the attainment of truly quantitative measures of blood hemodynamics within the microvasculature. This journey has involved numerous technical advancements and has been supported by several preclinical investigations and clinical translation examples. In the initial stages, LSI methods depended mainly on speckle contrast to yield information about the structural features of the vascular system, with limited details about the dynamic flow, which we classify as "qualitative techniques." Later, biophysics-based mathematical models were developed to extract flow-associated parameters using sample-specific assumptions, resulting in what we termed "semi-quantitative techniques." Lastly, fully quantitative LSI methods have been developed, which allow for longitudinal measurements without requiring the use of models or assumptions about the tissue, which may be inaccurate due to changes in tissue biophysical properties over time. Historically, these three classes of LSI approaches were developed sequentially (Figure 1).

The β parameter in the Siegert relationship is a dimensionless factor that relates the intensity autocorrelation function of the time-varying speckle pattern to the intensity contrast. It depends on the experimental setup, specifically the optical system's geometry, including considerations such as the illumination and detection unit, numerical aperture, and magnification of the imaging system. In LSI, the β parameter is critical because it can directly affect the calculated speckle contrast and consequently the estimated blood flow. Its value is typically assumed to be constant across an image, and is often chosen empirically to provide the best agreement with a gold-standard measurement, or based on theoretical considerations. However, variations in the β values, resulting from changes in the optical properties of tissues or alternations in the experimental setup, can introduce errors in blood flow measurements [44,118]. Therefore, in semi-quantitative techniques such as MESI and DLSI, the value of β is computed to measure the movement of scatterers directly.

Despite improvements relative to qualitative techniques, the semi-quantitative approaches still have limitations. Their output such as blood velocity needs to be standardized because variations in calibration techniques and potentially inaccurate underlying assumptions can affect the derived output. With such shortcomings, semi-quantitative techniques may not be well suited for longitudinal studies as they require calibration at each time point, limiting their ability to effectively compare blood

velocity maps across time. As such, they can only be used for effective comparisons among regions of interest within a particular field of view. On the other hand, the recently developed quantitative techniques do not need calibration nor rely on questionable biophysical assumptions. These can then enable meaningful longitudinal studies of blood hemodynamics, an exciting prospect to be undertaken by the LSI research community. However, in order to enable clinical applications, it is necessary to make further technical advancements and conduct preclinical trials to expand the fields of view and increase sensitivity to slow-flow-microvessels velocity maps.

To date, most clinical applications of LSI rely on the oldest approaches, such as qualitative techniques (Figure 4 and Table 2). Qualitative LSI has been extensively developed with advanced and robust technology, including image post-processing and motion correction routines. As expected, both semi-quantitative and quantitative techniques are relatively new and necessitate further technological developments and preclinical validation prior to their clinical use. Their optics must also remain compact and simple to facilitate smooth integration into clinical settings. For semi-quantitative methods, standardized and simplified protocols for imaging calibration are necessary to enable meaningful quantification of hemodynamics. On the technology front, developing better cameras with higher dynamic range, faster speed, and smaller form factors will be crucial in supporting the clinical translation of all LSI methodologies and enhancing their potential benefits.

In the coming years, the advancements in camera sensor technology are expected to bring significant improvements to all LSI methods, particularly those that attempt to furnish quantitative microvascular flow parameters. Specifically, the relatively low quantum efficiency of current silicon-based sensors such as sCMOS in the near-infrared spectral region is expected to be improved [130]. LSI has the potential to gather improved subsurface microvascular information due to the greater depth of penetration of these wavelengths compared to the visible range. This may spur the search for technological solutions to make LSI more of a volumetric imaging technique with depth-resolved tomographic (or at least depth-weighted) capabilities; in this context, it may be necessary to consider spatial frequency-modulated imaging approaches [131]. Furthermore, the development of revolutionary camera technologies such as quantitative CMOS and dynamic vision sensors [132] will enable orders of magnitude increase in frame rates, boosting spatiotemporal resolution and allowing for enhanced visualization of the smallest microvessels including capillaries. Using laser diodes with high illumination stability and optical fibers instead of free space optics can simplify future LSI devices, reduce costs, increase compactness,

and improve robustness, making them more suitable for potential clinical deployment. With the various advancements and the progression toward quantitative hemodynamics, the future of LSI appears promising in scientific, technological, preclinical, and even clinical domains.

CONFLICT OF INTEREST STATEMENT
The authors declare no conflicts of interest.

DATA AVAILABILITY STATEMENT
Data sharing not applicable to this article as no datasets were generated or analysed during the current study.

ORCID
Muhammad Mohsin Qureshi https://orcid.org/0000-0003-0362-0144

REFERENCES
[1] G. Guven, M. P. Hilty, C. Ince, *Blood Purif.* **2020**, *49*, 143.
[2] B. Thomas, K. S. Sumam, *Proc. Technol.* **2016**, *24*, 339.
[3] P. Vaupel, F. Kallinowski, P. Okunieff, *Cancer Res.* **1989**, *49*, 6449.
[4] B. K. Wacker, T. S. Park, J. M. Gidday, *Stroke* **2009**, *40*, 3342.
[5] F. N. Doubal, P. E. Hokke, J. M. Wardlaw, *J. Neurol. Neurosurg. Psychiatry* **2009**, *80*, 158.
[6] E. Farkas, P. G. M. Luiten, *Prog. Neurobiol.* **2001**, *64*, 575.
[7] L. Buée, P. R. Hof, A. Delacourte, *Ann. N. Y. Acad. Sci.* **1997**, *826*, 7.
[8] C. B. Robbins, A. C. Thompson, P. K. Bhullar, H. Y. Koo, R. Agrawal, S. Soundararajan, S. P. Yoon, B. W. Polascik, B. L. Scott, D. S. Grewal, S. Fekrat, *JAMA Ophthalmol.* **2021**, *139*, 182.
[9] D. Lominadze, W. L. Dean, S. C. Tyagi, A. M. Roberts, *Acta Physiol.* **2010**, *198*, 1.
[10] A. S. Chung, J. Lee, N. Ferrara, *Nat. Rev. Cancer* **2010**, *10*, 505.
[11] M. A. MacLean, L. Kamintsky, E. D. Leck, A. Friedman, *Fluids Barriers CNS* **2020**, *17*, 1.
[12] L. Deban, C. Correale, S. Vetrano, A. Malesci, S. Danese, *Am. J. Pathol.* **2008**, *172*, 1457.
[13] D. A. Long, J. T. Norman, L. G. Fine, *Nat. Rev. Nephrol.* **2012**, *8*, 244.
[14] P. K. Upputuri, K. Sivasubramanian, C. S. K. Mark, M. Pramanik, *Biomed. Res. Int.* **2015**, *2015*, 783983.

[15] N. Allam, W. J. Zabel, V. Demidov, B. Jones, C. Flueraru, E. Taylor, I. A. Vitkin, *Sci. Rep.* **2022**, *12*, 6140.

[16] K. S. Park, J. G. Shin, M. M. Qureshi, E. Chung, T. J. Eom, *Sci. Rep.* **2018**, *8*, 11614. https://doi.org/10.1038/s41598-018-29975-6

[17] S. Sakadžić, E. Roussakis, M. A. Yaseen, E. T. Mandeville, V. J. Srinivasan, K. Arai, S. Ruvinskaya, A. Devor, E. H. Lo, S. A. Vinogradov, D. A. Boas, *Nat. Methods* **2010**, *7*, 755.

[18] F. Helmchen, W. Denk, *Nat. Methods* **2005**, *2*, 932.

[19] V. Rajan, B. Varghese, T. G. van Leeuwen, W. Steenbergen, *Lasers Med. Sci.* **2009**, *24*, 269.

[20] S. Hu, L. v. Wang, *J. Biomed. Opt.* **2010**, *15*, 011101.

[21] K. Kim, K. Choe, I. Park, P. Kim, Y. Park, *Sci. Rep.* **2016**, *6*, 084.

[22] R. Alvarez-Román, A. Naik, Y. N. Kalia, H. Fessi, R. H. Guy, *Eur. J. Pharm. Biopharm.* **2004**, *58*, 301.

[23] K. D. Mac, M. M. Qureshi, M. Na, S. Chang, T. J. Eom, H. S. Je, Y. R. Kim, H.-S. Kwon, E. Chung, *Opt. Express* **2022**, *30*, 152.

[24] J. Senarathna, A. Rege, N. Li, N. V. Thakor, *IEEE Rev. Biomed. Eng.* **2013**, *6*, 99.

[25] D. A. Boas, A. K. Dunn, *J. Biomed. Opt.* **2010**, *15*, 011109.

[26] Y. Li, J. Chen, Z. Chen, *Transl. Biophotonics* **2019**, *1*, e201900005.

[27] R. J. Adrian, C. S. Yao, *Exp. Fluids* **1986**, *5*, 17.

[28] I. Aditya, V. Tat, A. Sawana, A. Mohamed, R. Tuffner, T. Mondal, *J. Neonatal. Perinatal. Med.* **2016**, *9*, 117.

[29] E. Bou, E. Bou, A. Ly, J. Roul, O. Llopis, C. Vieu, A. Cerf, *Biomed. Opt. Express* **2019**, *10*, 5862.

[30] H. Ishida, T. Andoh, S. Akiguchi, H. Shirakawa, D. Kobayashi, Y. Kuraishi, T. Hachiga, *Appl. Phys. Lett.* **2010**, *97*, 103702. https://doi.org/10.1063/1.3486678

[31] A. Ustione, D. W. Piston, *J. Microsc.* **2011**, *243*, 221.

[32] E. E. Hoover, J. A. Squier, *Nat. Photonics* **2013**, *7*, 93.

[33] T. Durduran, A. G. Yodh, *Neuroimage* **2014**, *85*, 51.

[34] P. R. Hoskins, *Clin. Phys. Physiol. Meas.* **1990**, *11*, 1.

[35] A. P. Fan, H. Jahanian, S. J. Holdsworth, G. Zaharchuk, *J. Cereb. Blood Flow Metab.* **2016**, *36*, 842.

[36] R. C. Webb, Y. Ma, S. Krishnan, Y. Li, S. Yoon, X. Guo, X. Feng, Y. Shi, M. Seidel, N. H. Cho, J. Kurniawan, J. Ahad, N. Sheth, J. Kim, J. G. Taylor VI, T. Darlington, K. Chang, W. Huang, J. Ayers, A. Gruebele, R. M. Pielak, M. J. Slepian, Y. Huang, A. M. Gorbach, J. A. Rogers, *Sci. Adv.* **2015**, *1*, e1500701. https://doi.org/10.1126/sciadv.1500701

[37] A. Mariampillai, A. Cable, B. A. Standish, B. C. Wilson, E. H. Moriyama, I. A. Vitkin, J. Jiang, M. Khurana, M. K. K. Leung, N. R. Munce, V. X. D. Yang, *Opt. Lett.* **2008**, *33*, 1530.

[38] A. F. Fercher, J. D. Briers, *Opt. Commun.* **1981**, *37*, 326.

[39] H. Cheng, Q. Luo, S. Zeng, S. Chen, J. Cen, H. Gong, *J. Biomed. Opt.* **2003**, *8*, 559.

[40] S. M. S. Kazmi, A. B. Parthasarthy, N. E. Song, T. A. Jones, A. K. Dunn, *J. Cereb. Blood Flow Metab.* **2013**, *33*, 798.

[41] A. Nadort, R. G. Woolthuis, T. G. van Leeuwen, D. J. Faber, *Biomed. Opt. Express* **2013**, *4*, 2347.

[42] D. D. Postnov, J. Tang, S. Evren Erdener, K. Kılıç, D. A. Boas, *Sci. Adv.* **2020**, *6*.

[43] M. M. Qureshi, Y. Liu, K. D. Mac, M. Kim, A. M. Safi, E. Chung, *Optica* **2021**, *8*, 1092.

[44] J. W. Goodman, *Speckle Phenomena in Optics: Theory and Applications*, 2nd ed., SPIE Press Book, Bellingham, WA **2020**.

[45] H. M. Pedersen, *Opt. Commun.* **1974**, *12*, 156.

[46] S. J. Kirkpatrick, D. D. Duncan, E. M. Wells-Gray, *Opt. Lett.* **2008**, *33*, 2886.

[47] J. W. Goodman, *Statistical Optics*, John Wiley & Sons, Inc, Hoboken, NJ **2015**.

[48] A. B. Parthasarathy, W. J. Tom, A. Gopal, X. Zhang, A. K. Dunn, *Opt. Express* **2008**, *16*, 1975.

[49] M. M. Qureshi, K. Duy Mac, A. H. Kim, Y. R. Kim, E. Chung, *Curr. Opt. Photonics* **2021**, *5*, 351.

[50] J. D. Briers, A. F. Fercher, *Optics in Biomedical Sciences. Springer Series in Optical Sciences*, Springer, Berlin, Heidelberg, Germany **1982**, p. 158.

[51] J. D. Briers, A. F. Fercher, in *Proc. SPIE 0369, Max Born Centenary Conf.*, SPIE, Edinburgh, UK, **1983**, pp. 22–28.

[52] B. J. Berne, R. Pecora, *Dynamic Light Scattering: With Applications to Chemistry, Biology, and Physics*, John Wiley & Sons, Inc, New York **1976**.

[53] H.-J. Jeon, M. M. Qureshi, S. Y. Lee, J. D. Badadhe, H. Cho, E. Chung, *Sci. Rep.* **2019**, *9*, 514.

[54] J. W. Goodman, *Proc. IEEE* **1965**, *53*, 1688.

[55] M. M. Qureshi, J. Brake, H.-J. Jeon, H. Ruan, Y. Liu, A. M. Safi, T. J. Eom, C. Yang, E. Chung, *Biomed. Opt. Express* **2017**, *8*, 4855.

[56] J. D. Briers, S. Webster, *J. Biomed. Opt.* **1996**, *1*, 174.

[57] J. D. Briers, P. M. McNamara, M. L. O'Connell, M. J. Leahy, in *Microcirculation Imaging* (Ed: M. J. Leahy), Wiley-Blackwell, Weinham, Germany **2012**, p. 147.

[58] E. Du, S. Shen, S. P. Chong, N. Chen, *Biomed. Opt. Express* **2007**, *2020*, 11.

[59] A. Cho, C. Yeon, D. Kim, E. Chung, *J. Opt. Soc. Korea* **2016**, *20*, 88.

[60] A. K. Dunn, H. Bolay, M. A. Moskowitz, D. A. Boas, *J. Cereb. Blood Flow Metab.* **2001**, *21*, 195.

[61] P. Li, S. Ni, L. Zhang, S. Zeng, Q. Luo, *Opt. Lett.* **2006**, *31*, 1824.

[62] P. Zakharov, A. Völker, M. Wyss, F. Haiss, N. Calcinaghi, C. Zunzunegui, A. Buck, F. Scheffold, B. Weber, *Opt. Express* **2009**, *17*, 904.

[63] M. S. Mahmud, D. W. Cadotte, B. Vuong, C. Sun, T. W. H. Luk, A. Mariampillai, V. X. D. Yang, *J. Biomed. Opt.* **2013**, *18*, 050901.

[64] A. Mariampillai, M. K. K. Leung, M. Jarvi, B. A. Standish, K. Lee, B. C. Wilson, A. Vitkin, V. X. D. Yang, *Opt. Lett.* **2010**, *35*, 1257.

[65] W. J. Zabel, N. Allam, W. D. Foltz, C. Flueraru, E. Taylor, I. A. Vitkin, *Sci. Rep.* **2022**, *12*, 3159.

[66] J. K. Meisner, J. Niu, S. Sumer, R. J. Price, *J. Biomed. Opt.* **2013**, *18*, 096011.

[67] D. Y. Li, Q. Xia, T. T. Yu, J. T. Zhu, D. Zhu, *Light Sci. Appl.* **2021**, *10*, 1.

[68] J. Lu, M. Chen, D. Wen, S. Huang, Z. Zhang, P. Li, S. Gui, *Opt. Lett.* **2018**, *43*, 5627.

[69] Y. Kim, W. J. Choi, J. Oh, J. K. Kim, *Biosensors* **2022**, *12*, 398.

[70] S. Lee, J. M. Namgoong, Y. Kim, J. Cha, J. K. Kim, *IEEE Trans. Biomed. Eng.* **2022**, *69*, 443.

[71] C.-Y. Lee, B.-H. Huang, W.-J. Chen, J.-Y. Yi, J.-Y. Yi, M.-T. Tsai, M.-T. Tsai, M.-T. Tsai, *OSA Contin.* **2020**, *3*, 1129.

[72] N. Hecht, J. Woitzik, J. P. Dreier, P. Vajkoczy, *Neurosurg. Focus* **2009**, *27*, E11.

[73] S. Eriksson, J. Nilsson, G. Lindell, C. Sturesson, *Med. Devices: Evid. Res.* **2014**, *7*, 261.

[74] S. Kojima, T. Sakamoto, Y. Nagai, Y. Matsui, K. Nambu, K. Masamune, *Surg. Innov.* **2019**, *26*, 293.

[75] V. Kalchenko, D. Israeli, Y. Kuznetsov, I. Meglinski, A. Harmelin, *J. Biophotonics* **2015**, *8*, 897.

[76] V. Kalchenko, A. Sdobnov, I. Meglinski, Y. Kuznetsov, G. Molodij, A. Harmelin, *Photonics* **2019**, *6*, 80.

[77] S. Yuan, A. Devor, D. A. Boas, A. K. Dunn, *Appl. Opt.* **2005**, *44*, 1823.

[78] E. Morales-Vargas, H. Peregrina-Barreto, J. C. Ramirez-San-Juan, *Comput. Methods Programs Biomed.* **2021**, *212*, 486.

[79] A. Völker, P. Zakharov, B. Weber, F. Buck, F. Scheffold, C. Ayata, Y. Ozdemir, A. Dunn, D. N. Atochin, P. L. Huang, V. R. Muzykantov, J. C. Murciano, D. A. Boas, M. A. Moskowitz, *Opt. Express* **2005**, *13*, 9782.

[80] J. Guilbert, M. Desjardins, *J. Biophotonics* **2022**, *15*, e202100218.

[81] X. Ma, A. Wang, F. Ma, S. Wu, H. Ming, Q. Zhan, *IEEE Access* **2020**, *8*, 499.

[82] W. J. Tom, A. Ponticorvo, A. K. Dunn, *IEEE Trans. Med. Imaging* **2008**, *27*, 1728.

[83] H. Kunikata, T. Nakazawa, *Asia Pac. J. Ophthalmol.* **2016**, *5*, 151.

[84] F. Nitta, H. Kunikata, N. Aizawa, K. Omodaka, Y. Shiga, M. Yasuda, T. Nakazawa, *Clin. Ophthalmol.* **2014**, *8*, 1127.

[85] E. Molnár, B. Molnár, Z. Lohinai, Z. Tóth, Z. Benyó, L. Hricisák, P. Windisch, J. Vág, *Biomed. Res. Int.* **2017**, *2017*, 4042902. https://doi.org/10.1155/2017/4042902

[86] S. M. White, M. Valdebran, K. M. Kelly, B. Choi, *Sci. Rep.* **2018**, *8*, 1.

[87] R. Farraro, O. Fathi, B. Choi, *J. Biomed. Opt.* **2016**, *21*, 094001.

[88] N. Hecht, J. Woitzik, S. König, P. Horn, P. Vajkoczy, *J. Cereb. Blood Flow Metab.* **2013**, *33*, 1000.

[89] R. Ambrus, L. B. Svendsen, N. H. Secher, K. Rünitz, H. J. Frederiksen, M. B. S. Svendsen, M. Siemsen, S. C. Kofoed, M. P. Achiam, *Scand. J. Gastroenterol.* **2017**, *52*, 455.

[90] R. C. Bray, K. R. Forrester, J. Reed, C. Leonard, J. Tulip, *J. Orthop. Res.* **2006**, *24*, 1650.

[91] N. Aizawa, H. Kunikata, F. Nitta, T. Nakazawa, *Acta Ophthalmol.* **2015**, *93*, e397.

[92] Y. Tamaki, M. Araie, E. Kawamoto, S. Eguchi, H. Fujii', *Invest. Ophthalmol. Vis. Sci.* **1994**, *35*, 3825.

[93] Y. Tamaki, M. Araie, K. Tomita, M. Nagahara, A. Tomidokoro, H. Fujii, *Jpn. J. Ophthalmol.* **1997**, *41*, 49.

[94] A. I. Srienc, Z. L. Kurth-Nelson, E. Newman, *Front. Neuroenergetics* **2010**, *2*, 128.

[95] A. Rege, S. I. Cunningham, Y. Liu, K. Raje, S. Kalarn, M. J. Brooke, L. Schocket, S. Scott, A. Shafi, L. Toledo, O. J. Saeedi, *Transl. Vis. Sci. Technol.* **2018**, *7*, 7.

[96] J. P. Borges, A. R. Nascimento, G. O. Lopes, D. J. M. Medeiros-Lima, M. P. Coelho, P. M. C. Nascimento, D. A. Kopiler, C. Matsuura, M. F. F. Mediano, E. Tibirica, *Clin. Physiol. Funct. Imaging* **2018**, *38*, 840.

[97] I. Cordovil, G. Huguenin, G. Rosa, A. Bello, O. Köhler, R. de Moraes, E. Tibiriçá, *Microvasc. Res.* **2012**, *83*, 376.

[98] A. Chizari, M. J. Schaap, T. Knop, Y. E. Boink, M. M. B. Seyger, W. Steenbergen, *Sci. Rep.* **2021**, *11*, 1.

[99] M.-E. Alexandrou, E. Gkaliagkousi, C. Loutradis, C. Dimitriadis, E. Mitsopoulos, A. Lazaridis, B. Nikolaidou, P. Dolgiras, S. Douma, A. Papagianni, P. A. Sarafidis, *Clin. Kidney J.* **2021**, *14*, 1419.

[100] A. Lazaridis, A. Triantafyllou, K. Dipla, P. Dolgyras, N. Koletsos, P. Anyfanti, S. Aslanidis, S. Douma, E. Gkaliagkousi, *Hypertens. Res.* **2021**, *45*, 445.

[101] B. Ruaro, A. Sulli, E. Alessandri, C. Pizzorni, G. Ferrari, M. Cutolo, *Ann. Rheum. Dis.* **2014**, *73*, 1181.

[102] D. P. Orgill, *NEJM* **2009**, *360*, 893.

[103] D. R. Miller, R. Ashour, C. T. Sullender, A. K. Dunn, in *Proc. SPIE 11945, Clinical and Translational Neurophotonics 2022*, SPIE, Bellingham, WA, 2022, p. 1194502.

[104] P. Hu, B. Niu, H. Yang, Y. Xia, D. Chen, C. Meng, K. Chen, B. Biswal, *Microcirculation* **2022**, *29*, e12783.

[105] M. J. Niemann, J. P. Eiberg, H. Sørensen, N. H. Secher, *J. Clin. Monit. Comput.* **2021**, *35*, 1263.

[106] S. Nomura, T. Inoue, H. Ishihara, H. Koizumi, E. Suehiro, F. Oka, M. Suzuki, *World Neurosurg.* **2014**, *82*, e753.

[107] A. M. Deana, S. H. C. Jesus, N. H. Koshoji, S. K. Bussadori, M. T. Oliveira, *Laser Phys.* **2013**, *23*, 075607.

[108] N. H. Koshoji, S. K. Bussadori, C. C. Bortoletto, R. A. Prates, M. T. Oliveira, A. M. Deana, *PLoS One* **2015**, *10*, e0118429.

[109] C. A. Nader, F. Pellen, H. Loutfi, R. Mansour, B. le Jeune, G. le Brun, M. Abboud, *J. Biomed. Opt.* **2015**, *21*, 071103.

[110] Q. Wu, J. Liu, B. Xu, W. Zhou, C. Wang, X. Yang, D. Xiong, *AIP Adv.* **2021**, *11*, 015031.

[111] C. Yi, J. Jung, J. Im, K. C. Lee, E. Chung, E. Chung, S. A. Lee, *Optica* **2022**, *9*, 1227.

[112] L. M. Richards, S. S. Kazmi, K. E. Olin, J. S. Waldron, D. J. Fox, A. K. Dunn, *J. Cereb. Blood Flow Metab.* **2017**, *37*, 3097.

[113] C. T. Sullender, L. M. Richards, F. He, L. Luan, A. K. Dunn, *J. Neurosci. Methods* **2022**, *366*, 434.

[114] T. Dragojević, D. Bronzi, H. M. Varma, C. P. Valdes, C. Castellvi, F. Villa, A. Tosi, C. Justicia, F. Zappa, T. Durduran, *Biomed. Opt. Express* **2015**, *6*, 2865.

[115] A. Nadort, K. Kalkman, T. G. Van Leeuwen, D. J. Faber, *Sci. Rep.* **2016**, *6*, 25258.

[116] Z. Turek, V. Černý, R. Pařízková, *Physiol. Res.* **2008**, *57*, 365.

[117] N. Bosschaart, G. J. Edelman, M. C. G. Aalders, T. G. van Leeuwen, D. J. Faber, *Lasers Med. Sci.* **2014**, *29*, 453.

[118] R. Bandyopadhyay, A. S. Gittings, S. S. Suh, P. K. Dixon, D. J. Durian, *Rev. Sci. Instrum.* **2005**, *76*, 093110.

[119] R. J. Adrian, *Annu. Rev. Fluid Mech.* **1991**, *23*, 261.

[120] R. D. Keane, R. J. Adrian, *Appl. Sci. Res.* **1992**, *49*, 191.

[121] K. Long, J. Liu, S. Shen, M. Thong, D. Wang, N. Chen, *Comput. Struct. Biotechnol. J.* **2023**, *21*, 1661.

[122] P. Strnad, S. Gunther, J. Reichmann, U. Krzic, B. Balazs, G. de Medeiros, N. Norlin, T. Hiiragi, L. Hufnagel, J. Ellenberg, *Nat. Methods* **2016**, *13*, 139.

[123] C. Ringers, E. W. Olstad, N. Jurisch-Yaksi, *Philos. Trans. R. Soc. B* **2020**, *375*, 20190156. https://doi.org/10.1098/rstb.2019.0156

[124] W. Thielicke, R. Sonntag, *J. Open Res. Softw.* **2021**, *9*, 12.

[125] A. Sdobnov, A. Bykov, G. Molodij, V. Kalchenko, T. Jarvinen, A. Popov, K. Kordas, I. Meglinski, *J. Phys. D: Appl. Phys.* **2018**, *51*, 155401.

[126] I. Stebakov, E. Kornaeva, D. Stavtsev, E. Potapova, V. Dremin, *Vib. Proced.* **2021**, *38*, 50.

[127] C. Millet, M. Roustit, S. Blaise, J. L. Cracowski, *Microvasc. Res.* **2011**, *82*, 147.

[128] A. Humeau-Heurtier, P. Abraham, G. Mahe, *IEEE Trans. Med. Imaging* **2013**, *32*, 2311.

[129] V. Kalchenko, D. Israeli, Y. Kuznetsov, A. Harmelin, *Sci. Rep.* **2014**, *4*, 5839.

[130] K. D. Stefanov, *CMOS Image Sensors*, IOP Publishing, Bristol, UK **2022**.

[131] N. Worts, J. Field, R. Bartels, J. Jones, J. Broderick, J. Squier, *Opt. Lett.* **2018**, *43*, 5351.

[132] Hamamatsu Photonics, *ORCA-Quest qCMOS Camera C15550-20UP*, https://www.hamamatsu.com/us/en/product/cameras/qcmos-cameras/C15550-20UP.html (accessed: Febraury 2023).

AUTHOR BIOGRAPHIES

Muhammad Mohsin Qureshi completed his master's (M.S.) in Photonics Engineering from Chosun University, South Korea (March 2014–February 2016). He received his Ph.D. degree in Biomedical Engineering from Gwangju Institute of Science and Technology (GIST), South Korea with specialization in Biophotonics (September 2016–August 2021). Currently, he is a postdoctoral researcher at the University Health Network since November 2021. His research interests include biomedical optics, laser speckle imaging, optical coherence tomography, and their applications.
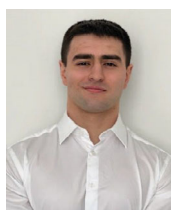
Nader Allam completed his B.Sc. with specialized Honors in Biophysics from York University, Canada (September 2015–August 2019). He recently graduated with his M.Sc. in Medical Biophysics from the University of Toronto, Canada (September 2019–January 2023). His research interests include biomedical optics and its applications, radiation biology and physics, prosthetics engineering, and the fields of emergency, internal and neurorehabilitation medicine.
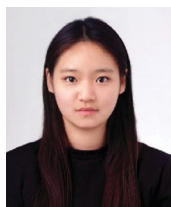
Jeongmyo Im graduated from Konkuk University with a degree in biotechnology in 2021. During her undergraduate years, she spent time as a student researcher at the Biooptics Lab. She completed her master's (M.S.) from Gwangju Institute of Science and Technology (GIST), South Korea with specialization in Neurophotonics in 2023 and is currently pursuing a Ph. D. focusing on laser speckle imaging and its application.

Hyuk-Sang Kwon is an associate professor in the biomedical science and engineering department at GIST. He holds a B.S. from the University of Iowa, and an M.S. and Ph.D. in mechanical engineering from MIT. Dr. Kwon served as a lab instructor in the MIT department of biological engineering before establishing his research lab, 3D-BIT. His lab focuses on utilizing optical technologies to develop cutting-edge medical devices and explore new aspects of life phenomena. His research interests include the development of a light-tissue interaction simulation tool, the application of holography on biological imaging, and the creation of 3D imaging analysis tools.

Euiheon Chung is a professor in the biomedical science and engineering department at Gwangju Institute of Science and Technology and the director of the Gliopathic Pain Research Center. He graduated from KAIST with M.S. and B.S. in aerospace engineering with a minor in physics. He received Ph.D. from the Harvard-MIT Division of Health Sciences and Technology (HST) at MIT, followed by postdoc at Massachusetts General Hospital and Harvard Medical School. He aims to create translational neurophotonic technologies to satisfy unmet clinical needs based on biomedical engineering approaches, especially in functional optical imaging and neuromodulation.

I. Alex Vitkin is a professor of Medical Biophysics and Radiation Oncology at the University of Toronto, a senior scientist at the University Health Network, and a clinical medical physicist at Princess Margaret Cancer Centre. He has published over 190 papers and book chapters on biomedical optics, specializing in tissue polarimetry and functional optical coherence tomography. He has delivered special seminars and summer school modules on biophotonics in 26 countries, often through SPIE's and Optica's International Visiting Lecturer programs. Dr. Vitkin is a Fellow of Optica, SPIE, and AIMBE, and is the 2022 recipient of the SPIE GG Stokes Award in optical polarization.